

Auto DragGAN: Editing the Generative Image Manifold in an Autoregressive Manner

Pengxiang Cai
 Foundation Model Research Center,
 Institute of Automation, Chinese
 Academy of Sciences
 Beijing, China
 School of Artificial Intelligence,
 University of Chinese Academy of
 Sciences
 Beijing, China
 Wuhan AI Research
 Wuhan, China
 caipengxiang2022@ia.ac.cn

Zhiwei Liu*
 Foundation Model Research Center,
 Institute of Automation, Chinese
 Academy of Sciences
 Beijing, China
 School of Artificial Intelligence,
 University of Chinese Academy of
 Sciences
 Beijing, China
 Wuhan AI Research
 Wuhan, China
 zhiwei.liu@nlpr.ia.ac.cn

Guibo Zhu*
 Foundation Model Research Center,
 Institute of Automation, Chinese
 Academy of Sciences
 Beijing, China
 School of Artificial Intelligence,
 University of Chinese Academy of
 Sciences
 Beijing, China
 Wuhan AI Research
 Wuhan, China
 gbzhu@nlpr.ia.ac.cn

Yunfang Niu
 Foundation Model Research Center,
 Institute of Automation, Chinese
 Academy of Sciences
 Beijing, China
 School of Artificial Intelligence,
 University of Chinese Academy of
 Sciences
 Beijing, China
 Wuhan AI Research
 Wuhan, China
 niuyunfang2019@ia.ac.cn

Jinqiao Wang
 Foundation Model Research Center,
 Institute of Automation, Chinese
 Academy of Sciences
 Beijing, China
 School of Artificial Intelligence,
 University of Chinese Academy of
 Sciences
 Beijing, China
 Peng Cheng Laboratory
 Shenzhen, China
 Wuhan AI Research
 Wuhan, China
 jqwang@nlpr.ia.ac.cn

Abstract

Pixel-level fine-grained image editing remains an open challenge. Previous works fail to achieve an ideal trade-off between control granularity and inference speed. They either fail to achieve pixel-level fine-grained control, or their inference speed requires optimization. To address this, this paper for the first time employs a regression-based network to learn the variation patterns of StyleGAN latent codes during the image dragging process. This method enables pixel-level precision in dragging editing with little time cost. Users can specify handle points and their corresponding target points on any GAN-generated images, and our method will move each handle point to its corresponding target point. Through

experimental analysis, we discover that a short movement distance from handle points to target points yields a high-fidelity edited image, as the model only needs to predict the movement of a small portion of pixels. To achieve this, we decompose the entire movement process into multiple sub-processes. Specifically, we develop a transformer encoder-decoder based network named 'Latent Predictor' to predict the latent code motion trajectories from handle points to target points in an autoregressive manner. Moreover, to enhance the prediction stability, we introduce a component named 'Latent Regularizer', aimed at constraining the latent code motion within the distribution of natural images. Extensive experiments demonstrate that our method achieves state-of-the-art (SOTA) inference speed and image editing performance at the pixel-level granularity.

*Corresponding author.

Permission to make digital or hard copies of all or part of this work for personal or classroom use is granted without fee provided that copies are not made or distributed for profit or commercial advantage and that copies bear this notice and the full citation on the first page. Copyrights for components of this work owned by others than the author(s) must be honored. Abstracting with credit is permitted. To copy otherwise, or republish, to post on servers or to redistribute to lists, requires prior specific permission and/or a fee. Request permissions from permissions@acm.org.

MM '24, October 28–November 1, 2024, Melbourne, Australia

© 2024 Copyright held by the owner/author(s). Publication rights licensed to ACM.
 ACM ISBN 978-1-4503-XXXX-X/18/06
<https://doi.org/XXXXXXXX.XXXXXXX>

CCS Concepts

• **Computing methodologies** → **Computer vision; Image manipulation.**

Keywords

GANs, Image Editing, Autoregressive Model

ACM Reference Format:

Pengxiang Cai, Zhiwei Liu, Guibo Zhu, Yunfang Niu, and Jinqiao Wang. 2024. Auto DragGAN: Editing the Generative Image Manifold in an Autoregressive Manner. In *Proceedings of Make sure to enter the correct conference title from your rights confirmation email (MM '24)*. ACM, New York, NY, USA, 9 pages. <https://doi.org/XXXXXXX.XXXXXXX>

1 Introduction

Significant advances [8, 11, 18, 32] in the field of image generation have also fostered research in image editing. Images obtained by generative models [13–15, 26] can now satisfy the needs of most users, yet they lack flexible and free control. Editing [16, 22] images generated by these models can provide users with the flexible and free control they desire, thereby enabling them to obtain images that meet their specific requirements. Image editing methods based on generative models have attracted widespread attention among researchers. However, fine-grained control in image editing remains an open challenge, especially at the pixel level. Previous research [2, 10, 16, 20, 22, 23, 25] has failed to achieve an ideal trade-off between control granularity and inference time. They either failed to achieve pixel-level fine-grained control, or their inference speed required optimization. Numerous methods [10, 16, 20, 23] enable image editing based on text prompts, with editing operations including replacing image subjects, modifying subject poses, and altering image styles. Additionally, PTI [25] leverages attribute labels to guide StyleGAN [12–15] in modifying specific attributes of images, such as facial expressions, face orientations, and the age of persons. Due to the limitations of text prompts and attribute labels in delivering fine-grained information, these methods are restricted to coarse-grained control. Currently, most research focuses on coarse-grained control, thus fine-grained image editing still has many problems to be investigated and solved.

Recently, DragGAN [22] has achieved an interactive image editing method based on pixel manipulation for the first time, which allows users to drag the image subject. This method has resulted in astonishing drag editing effects with pixel-level precision. However, the principal idea of DragGAN [22] is the iterative reverse optimization of latent codes in the StyleGAN [12–15] space, which requires enhancement in computational efficiency.

Overall, previous research has failed to achieve an ideal trade-off between control granularity and inference speed. They either fail to achieve pixel-level fine-grained control, or their inference speed requires optimization. To do this, this paper introduces a regression based network for learning the variation patterns of latent codes within the StyleGAN [12–15] space during the image dragging process, thereby achieving pixel-level precision in drag editing with little time cost. Compared to UserControllableLT [6], our method achieves pixel-level fine-grained control. In comparison with DragGAN [22], our approach achieves a comparable level of fine-grained control while significantly reducing the required inference time. As illustrated in Figure 1, our method achieves an ideal trade-off between control granularity and inference speed. Extensive experiments demonstrate that our method achieves state-of-the-art (SOTA) inference speed and image editing performance at the pixel-level granularity.

We develop a transformer encoder-decoder based network named 'Latent Predictor' to predict the latent code motion trajectories from

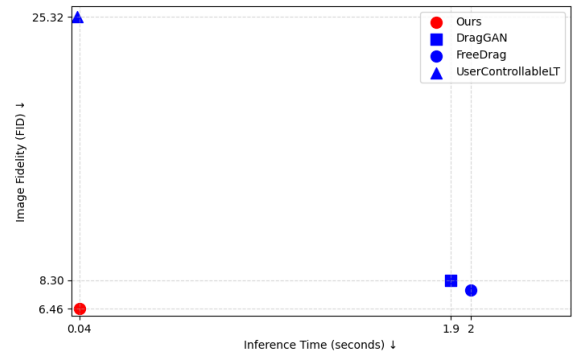


Figure 1: The comparison between UserControllableLT [6], DragGAN [22], FreeDrag [19] and our proposed Auto DragGAN in terms of key performance indicators. Inference time (seconds) ↓ and image fidelity (FID) ↓ were both tested in the face landmark manipulation experiment under the settings described in Section 4.3.1, based on the 'one point' setting.

handle points to target points in an autoregressive manner. Moreover, to enhance the prediction stability, we introduce a component named 'Latent Regularizer', aimed at constraining the latent code motion within the distribution of natural images.

Specifically, we propose a two-stage training strategy. In the first stage, we introduce the Latent Regularizer to constrain the latent code motion, ensuring that the latent code remains within the reasonable distribution of the StyleGAN [12–15] latent space to enhance the stability of the Latent Predictor. By introducing random noise to the latent codes, we generate outlier latent codes that fall outside the reasonable distribution of the StyleGAN [12–15] latent space. Subsequently, we train the Latent Regularizer utilizing an attention mechanism to learn the internal structural information within the latent code, thereby correcting outlier latent codes back within the reasonable distribution of the StyleGAN [12–15] latent space.

In the second stage of training, we have developed a network based on the transformer encoder-decoder architecture, which we refer to as the 'Latent Predictor'. This network effectively converts the image drag problem [22] into a latent code motion sequences regression task. It is jointly trained with the Latent Regularizer to regularize the prediction results. Initially, to obtain pseudo-labels for training, we introduce continuous and slight random noise into the randomly sampled latent codes to generate latent code motion sequences. These motion sequences simulate a 'pseudo-process' to approximate the actual dragging process. The Latent Predictor autoregressively predicts this 'pseudo-process', employing a cross-attention mechanism to learn the motion trajectories from handle points to target points, thereby precisely moving the handle points to their corresponding target points.

In summary, the three principal contributions of this paper are as follows: (1) For the first time, we present a regression-based network that achieves pixel-level fine-grained image editing; (2) We convert the image dragging problem into a regression problem

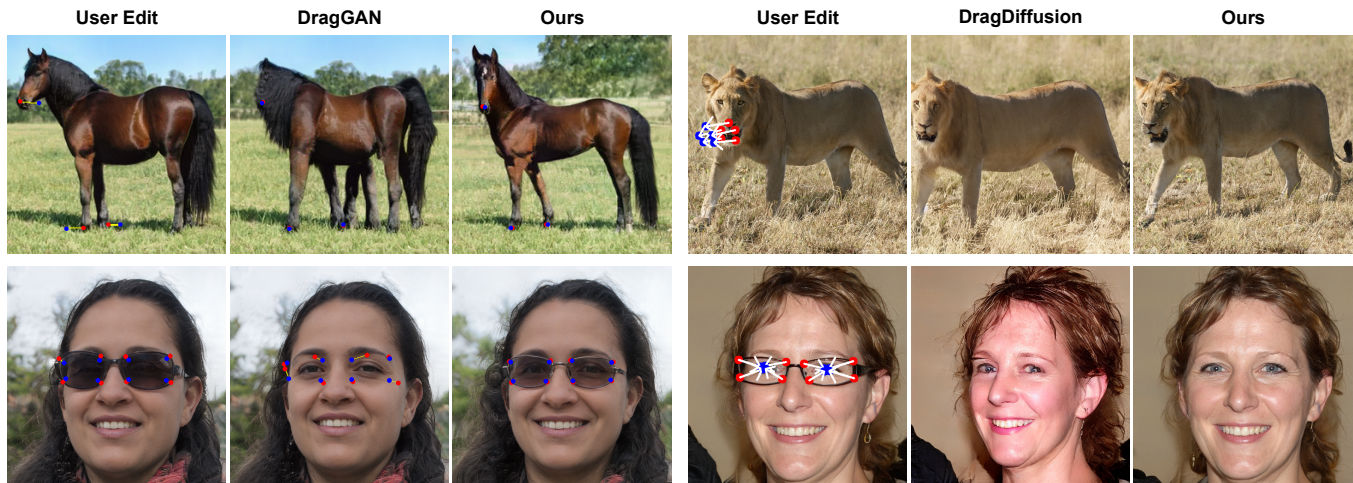


Figure 2: Users are able to specify handle points (marked as red) and target points (marked as blue) on any GAN-generated images, and our method will precisely move the handle points to reach their corresponding target points, thereby achieving the desired drag effect on the image. We compare DragGAN [22] and DragDiffusion [27] with our proposed Auto DragGAN, which demonstrates superior drag performance.

of latent code motion sequences for the first time and propose a Latent Regularizer as well as a Latent Predictor based on a transformer encoder-decoder architecture; (3) Extensive experiments demonstrate the effectiveness and efficiency of our method, which achieves an ideal trade-off between control granularity and inference speed. Extensive experiments demonstrate that our method achieves state-of-the-art (SOTA) inference speed and image editing performance at the pixel-level granularity.

2 Related work

2.1 Image Generative Models

GANs. Generative Adversarial Networks (GANs) consist of two neural networks, a generator and a discriminator, that work in tandem. The generator creates synthetic data, while the discriminator evaluates its authenticity. This adversarial process pushes the generator to produce increasingly realistic outputs [5, 8, 12–15]. Initial GAN models struggled with issues like unstable training and mode collapse. Deep Convolutional GANs (DCGANs) [24] improved the quality of generated images by using convolutional layers. A major advancement came with StyleGAN [12–15], which introduced a "style-based" generator architecture. This innovation allows for precise control over various aspects of the generated images, such as facial features and background details. StyleGAN2 [15] further refined this approach, enhancing image quality and consistency. These advancements have solidified GANs, particularly StyleGAN [12–15], as a powerful tool for image synthesis, data augmentation, and creative content generation.

Diffusion Models. Diffusion models [29] have significantly advanced image generation by mimicking thermodynamic diffusion processes. They use a two-step approach: a forward process that adds Gaussian noise to an image until it's unrecognizable, and a reverse process that progressively denoises it to regenerate the original or create a new coherent image. Early diffusion models faced

efficiency challenges, but the introduction of Denoising Diffusion Probabilistic Models (DDPMs) [11] marked a major breakthrough. DDPMs streamlined training and improved image quality, rivaling GANs by generating diverse, high-fidelity images while avoiding issues like mode collapse. Advancements include optimized noise scheduling and improved neural network architectures, enhancing model efficiency and scalability. Score-Based Generative Models (SGMs) [30, 31] further refined the approach using score matching, providing a more robust framework. Modern models are predominantly hybrid models [3, 9], with recent examples combining diffusion techniques with VAEs [18] and GANs, merging the stable training of diffusion models with the efficient sampling of other frameworks; these developments position diffusion models as a powerful and scalable alternative in the realm of image generation, promising high-quality synthetic images for various applications.

2.2 Pixel-Level Fine-Grained Image Editing

UserControllableLT [6] and DragGAN [22] are point-based editing methods that have been previously proposed. Particularly, DragGAN [22] allows users to input handle points and target points, enabling the dragging manipulation of images. Concurrent to our work are FreeDrag [19] and DragDiffusion [27]. FreeDrag [19] proposes a novel point-tracking-free paradigm to enhance DragGAN [22]. DragDiffusion [27] extends the editing framework of DragGAN [22] to diffusion models. DragGAN [22], FreeDrag [19], and DragDiffusion [27] are all methods based on the optimization of latent codes. Our proposed method differs significantly from all of these approaches.

3 Method

In this paper, we propose a novel regression-based network architecture that achieves fine-grained image editing at the pixel level. Given a source image and its handle points and target points, the

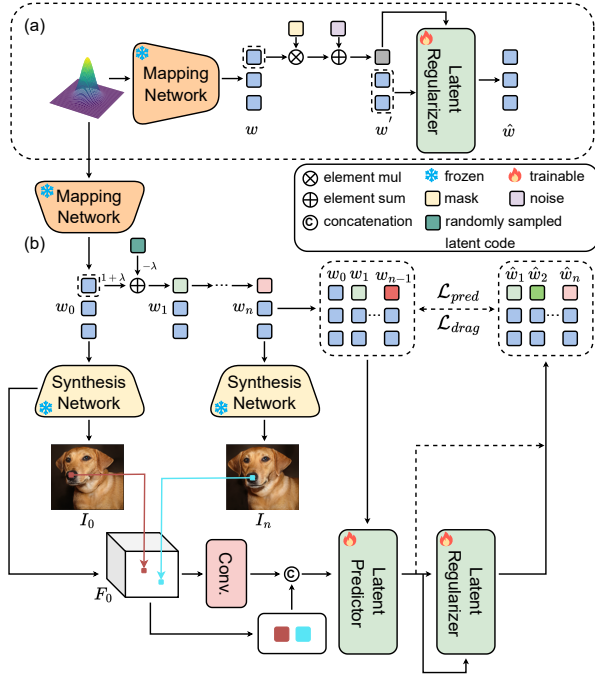


Figure 3: The overview of our proposed Auto DragGAN. (a) corresponds to the first stage of training, namely the pre-training of the Latent Regularizer. (b) represents the second stage of training, which is the joint training of the Latent Predictor and the Latent Regularizer.

network predicts the motion trajectories in the StyleGAN latent space to make the handle points reach their corresponding target point positions in image space. Initially, in Section 3.1, we introduce the Latent Regularizer, aimed at constraining the latent code motion within a reasonable range. In Section 3.2, the Latent Predictor, which is employed to predict the latent code motion sequences, is discussed.

3.1 Latent Regularizer

Our training process is divided into two distinct stages. The first stage is dedicated to the pre-training of the Latent Regularizer, followed by the second stage which focuses on the joint training of both the Latent Predictor and the Latent Regularizer. This section will detail the training conducted during the first stage as well as the proposed Latent Regularizer.

As illustrated in Figure 4, due to the complex distribution of the \mathcal{W}^+ space, even minor inference errors can generate outlier latent codes that fall outside the reasonable distribution of the \mathcal{W}^+ space. This can lead to a significant degradation in the fidelity of the generated images, which is manifested as artifacts or incorrect dragging in the pixel space. Therefore, we need to train an additional Latent Regularizer to ensure that the latent code motion remains within the reasonable distribution of the \mathcal{W}^+ space. This assists the Latent Predictor in more stably forecasting the latent code motion sequences.

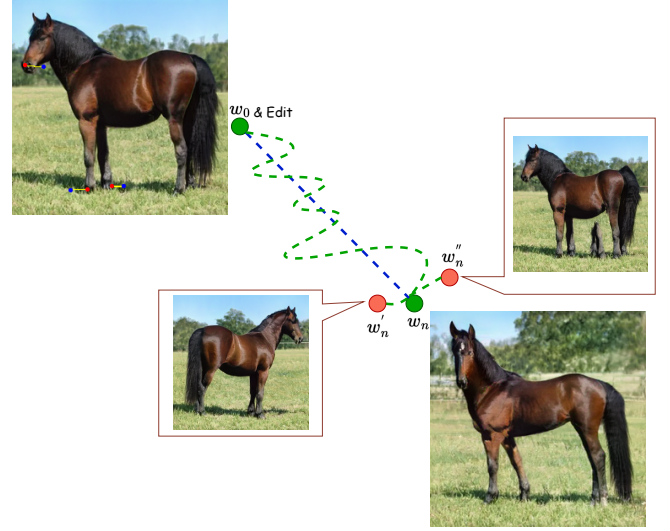


Figure 4: The outlier latent codes. The shortest motion path in the \mathcal{W}^+ space between the latent code w_0 and its edited result w_n is depicted as the blue dashed line in the figure, while the green dashed line represents the motion trajectory learned by our model. w'_n and w''_n are the outlier latent codes, predicted by the model without the use of the Latent Regularizer.

As illustrated in Figure 3 (a), the mapping network of StyleGAN2 [15] randomly samples a 512-dimensional latent code z from a normal distribution and maps it to a latent code w of dimension $l \times 512$, where l represents the number of layers in the generator network. These mapped latent codes serve as training samples for the Latent Regularizer. UserControllableLT [6] finds that manipulating latent codes on deep layers enables spatial control, such as pose and orientation. DragGAN [22] considers the feature maps after the 6th block of StyleGAN2 [15], which performs the best among all features due to a good trade-off between resolution and discriminativeness. Inspired by UserControllableLT [6] and DragGAN [22], our work is based on the editing of the first six layers of the latent code w .

To obtain the outlier latent code, we introduce random noise to the randomly sampled latent code w . In the first stage of training, we initially add noise to the first six layers of w . Specifically, we perform a masking operation on the first six layers of w , randomly setting the vector values of these layers to zero with a 25% probability, followed by the addition of Gaussian noise.

$$w' = (w \odot M) + N \quad (1)$$

where w' represents the outlier latent code, \odot denotes the Hadamard product, M is the masking vector with elements being 0 or 1, and N is the noise sampled from a Gaussian distribution.

Prior work [6, 12–15, 22] finds that manipulating the first six layers of the latent codes enables spatial control, such as pose and orientation. Thus, w' is divided into two sets of vectors: the noisy vectors w'_1 from the first six layers and the remaining clean vectors w'_2 .

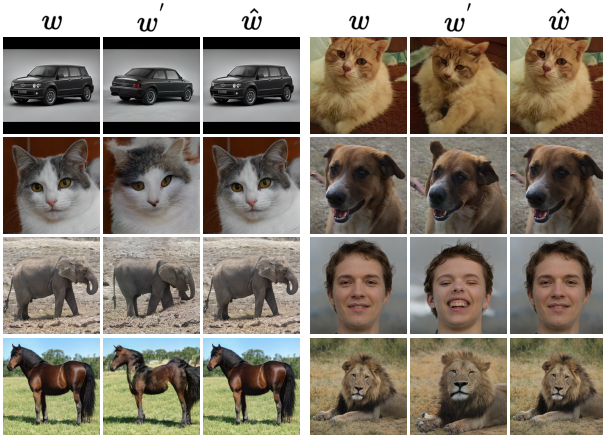


Figure 5: Reconstruction of the outlier latent codes. For each set of images, the first, second, and third columns correspond to the initial random sampled latent code w , the outlier latent code w' , and the reconstructed \hat{w} , respectively.

Given that w'_1 is more closely associated with local features, and w'_2 predominantly relates to global features [6, 12–15, 22], we aim to restore the noise-added local features w'_1 by leveraging the clean global features w'_2 .

The Latent Regularizer structure adopts a standard transformer architecture, with w'_1 serving as the key and value for the cross-attention mechanism, while w'_2 , after being mapped through an MLP to reduce token length, acts as the query for the cross-attention mechanism. The output of the cross-attention mechanism, serving as the restored local features, is concatenated with the clean global features w'_2 to form the reconstructed latent code \hat{w} .

$$q = Q \cdot (MLP(w'_2) \oplus PE) \quad (2)$$

$$k = K \cdot MLP(w'_1) \quad (3)$$

$$v = V \cdot MLP(w'_1) \quad (4)$$

$$\hat{w} = [(softmax(q \cdot k^T) \cdot v), w'_2] \quad (5)$$

where PE denotes the position embedding, \oplus denotes element-wise sum, and $[,]$ indicates the concatenation operation.

The Latent Regularizer learns to recover clean latent codes from noisy latent codes through a reconstruction task. The reconstruction loss is chosen to be the $L1$ Loss, with the latent code w serving as the label.

$$\mathcal{L}_{reg} = \mathbb{E}_{w \sim p(z)} \|\hat{w} - w\|_1 \quad (6)$$

As illustrated in Figure 5, the Latent Regularizer is capable of eliminating the random noise introduced into the latent codes, thereby correcting the outlier latent codes back into the reasonable distribution of the \mathcal{W}^+ space. Indeed, through the reconstruction task, the Latent Regularizer learns to (i) infer latent codes from their internal structure, and (ii) restore erroneous and missing data. This process facilitates the Latent Regularizer in learning the mapping representations of natural image prior distributions in the \mathcal{W}^+ space.

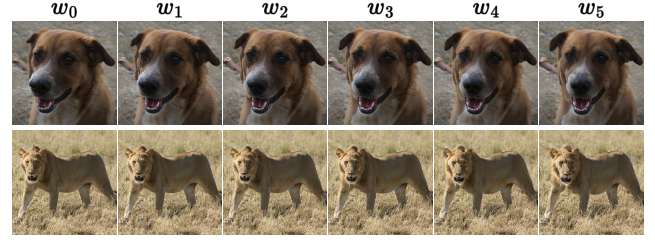


Figure 6: Visualization of the latent code motion sequence. Given an initial latent code w_0 , a sequence w_0, w_1, \dots, w_5 can be generated through the perturbation process described by Equation (7), where $i = 1, 2, 3, 4, 5$.

3.2 Latent Predictor

This section will elaborate on the proposed Latent Predictor, as well as the joint training of the Latent Predictor and the Latent Regularizer.

As illustrated in Figure 3 (b), the mapping network of StyleGAN2 [15] randomly samples a 512-dimensional latent code z from a normal distribution and maps it to a latent code w_0 of dimension $l \times 512$, where l represents the number of layers in the generator network. Subsequently, we slightly perturb the first six layers of w_0 to obtain w_1 , and then similarly perturb the first six layers of w_1 to acquire w_2 , and so forth. By repeating this process of minor random perturbations n times, we generate a sequence of latent codes $w_0, w_1, w_2, \dots, w_n$. The perturbation process is as follows:

$$w_i = w_{i-1} - \lambda \cdot (w^* - w_{i-1}) \quad (7)$$

where λ is a constant, w^* is an independently sampled latent code unrelated to w_0 , and $i = 1, 2, \dots, n$.

Prior work [6, 12–15, 22] finds that manipulating the first six layers of the latent codes enables spatial control, such as pose, orientation and shape. Our perturbation process does not affect other styles, such as color and texture. Therefore, our perturbation facilitates the preservation of identity information during the image dragging process. As illustrated in Figure 6, our perturbation process of latent codes in the StyleGAN2 [15] latent space corresponds to spatial variations in the pixel space of images, such as pose, orientation, and shape. Therefore, the sequence w_0, w_1, \dots, w_n is a latent code motion sequence. By utilizing this motion sequence as a training sample, the image dragging problem can be decomposed into multiple sequential sub-problems. Between two consecutive sub-problems, the majority of pixels in the images before and after dragging remain consistent, requiring the model to predict the movement of only a small portion of pixels, thereby significantly reducing the complexity of the problem.

The Latent Predictor employs a straightforward teacher-forcing cross-attention Transformer Decoder [33] for motion sequence prediction. The latent codes w_0 and w_n are processed through the StyleGAN2 generator network [15] to produce the synthesized images I_0 and I_n , respectively. An off-the-shelf feature matching algorithm [1] is applied to I_0 and I_n , with matching points whose pixel distance exceeds 50 selected as training sample points. The matching points of I_0 are designated as handle points (for instance, the red point of I_0 in Figure 3 (b)), and those of I_n as target points

(for instance, the **blue point** of I_n in Figure 3 (b)). DragGAN [22] focuses on the feature maps from the 6th block of StyleGAN2 [15], as they offer an optimal balance between resolution and discriminative power, outperforming other features in effectiveness. Inspired by DragGAN [22], we use the feature map obtained after passing w_0 through the 6th block of the StyleGAN2 [15] generator network as the intermediate feature map F_0 in our work. Subsequently, we extract small patches corresponding to the positions of handle points and target points on F_0 . After F_0 undergoes convolution to extract spatial information, it is concatenated with the small patches to serve as the key and value for the cross-attention mechanism. The sequence composed of w_0, w_1, \dots, w_{n-1} is combined with position embeddings through element-wise addition, serving as the query for the cross-attention mechanism. During training, teacher forcing is employed to predict $\hat{w}_1, \hat{w}_2, \dots, \hat{w}_n$. The final output is connected via skip connection to the Latent Regularizer, to constrain the predicted latent code motion sequences within the reasonable distribution of the \mathcal{W}^+ space.

$$k = K \cdot \text{MLP}([\text{MLP}(F_{seq}), \text{MLP}(P_{seq})]) \quad (8)$$

$$v = V \cdot \text{MLP}([\text{MLP}(F_{seq}), \text{MLP}(P_{seq})]) \quad (9)$$

$$q = Q \cdot (\text{MLP}([w_0; w_1; \dots; w_{n-1}]) \oplus PE) \quad (10)$$

$$[\hat{w}_1; \hat{w}_2; \dots; \hat{w}_n] = D(\text{MLP}(\text{softmax}(q \cdot k^T) \cdot v)) \quad (11)$$

where F_{seq} denotes the sequence of feature vectors extracted from the intermediate feature F_0 after spatial convolution to gather information, and P_{seq} represents the 7×7 patches at the positions corresponding to the handle points and target points on F_0 , and PE denotes the position embedding. The notation $[\cdot]$ is used to represent the formation of a latent code sequence, while $[\cdot]$ indicates the concatenation operation.

The Latent Predictor aims to learn the state transition path from w_0 to w_n , with the L1 loss function employed as the loss function.

$$\mathcal{L}_{pred} = \mathbb{E}_{w \sim p(z)} \|\hat{w}_{seq} - w_{seq}\|_1 \quad (12)$$

where \hat{w}_{seq} denotes the set consisting of $w_0, \hat{w}_1, \hat{w}_2, \dots, \hat{w}_n$, and w_{seq} represents the set containing $w_0, w_1, \dots, w_{n-1}, w_n$.

Furthermore, we apply a drag loss to the intermediate feature maps to guide the handle points towards the target points. Specifically, we use the feature of the handle patch before dragging as supervision for the feature of the target patch after dragging.

$$\mathcal{L}_{drag} = \sum_{i=0}^{n-1} \sum_{j=1}^{m_i} \sum_{\substack{h_{i,j} \in \Omega(H_{i,j}) \\ t_{i,j} \in \Omega(T_{i,j})}} \|F_i(h_{i,j}) - \hat{F}_{i+1}(t_{i,j})\|_1 \quad (13)$$

where n represents the length of the latent code motion sequence, and m_i is the number of matching points between the generated images I_i and I_{i+1} corresponding to w_i and w_{i+1} , with only matching points exceeding a pixel distance of 30 being selected. The matching points on I_i are designated as handle points $H_{i,j}$ (the **red point** of I_i in Figure 7), and those on I_{i+1} are designated as target points $T_{i,j}$ (the **blue point** of I_{i+1} in Figure 7). We use $\Omega(H_{i,j})$ to represent the pixels within a 7×7 patch centered at $H_{i,j}$. F_i and \hat{F}_{i+1} are the intermediate feature maps of w_i and \hat{w}_{i+1} , respectively. $F(h_{i,j})$ denotes the feature values of F at pixel $h_{i,j}$. This loss function encourages the handle points to move towards the target points.

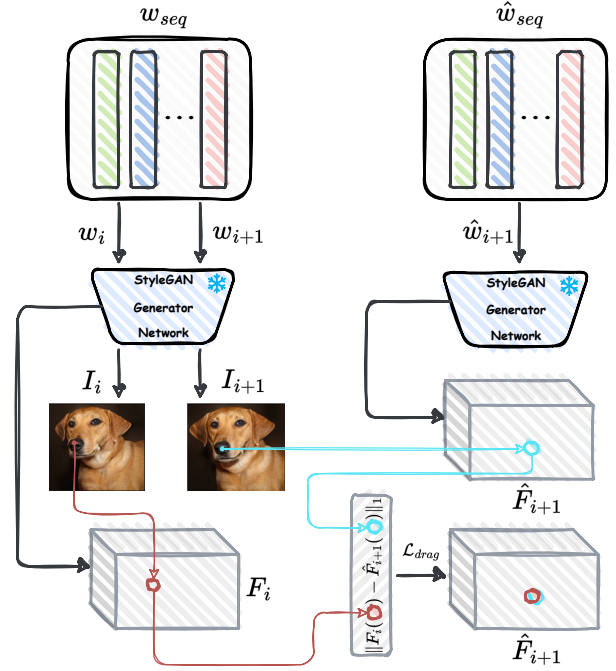


Figure 7: Drag Loss. The Drag loss supervises the patches of intermediate features to guide the handle points towards the target points.

Finally, the overall loss function is defined as:

$$\mathcal{L} = \alpha \mathcal{L}_{pred} + \beta \mathcal{L}_{drag} \quad (14)$$

where α and β are coefficients to balance the two loss functions, with α set to 0.1 and β set to 1 by default in our experiments.

4 Experiment

4.1 Training And Inference

Following the setup of DragGAN [22], we utilized the StyleGAN2 [15] pre-trained on the following datasets (the resolution of the pretrained StyleGAN2 [15] is shown in brackets): FFHQ (512) [14], AFHQCat (512) [4], SHHQ (512) [7], LSUN Car (512) [34], LSUN Cat (256) [34], Landscapes HQ (256) [28] and self-distilled dataset from Self-distilled stylegan [21] including Lion (512) [21], Dog (1024) [21], and Elephant (512) [21].

The Latent Regularizer employs a standard transformer architecture, consisting of a self-attention mechanism with 6 transformer encoder layers, and a cross-attention mechanism with 6 transformer decoder layers [33]. The Latent Predictor consists of a self-attention mechanism with 6 transformer encoder layers, and a cross-attention mechanism with 16 transformer decoder layers [33].

In the first stage of training, only Latent Regularizer requires training, with its learning rate set to 1×10^{-3} . In the second stage of training, both Latent Regularizer and Latent Predictor require joint training. The learning rate for Latent Regularizer is set at 1×10^{-5} , while Latent Predictor employs a cosine annealing decay for its

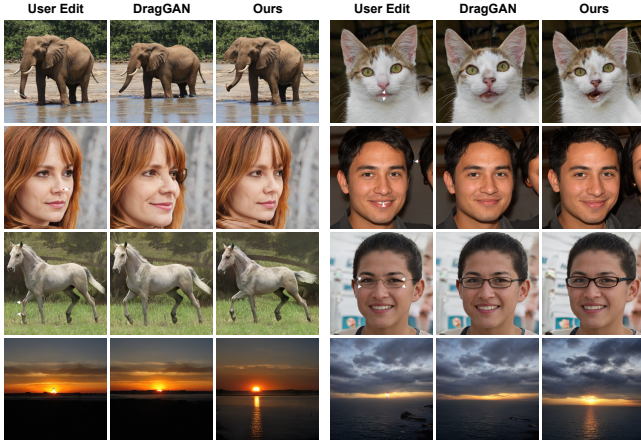


Figure 8: A qualitative comparison of the image editing performance between our method and DragGAN [22].

learning rate, with an initial value set at 1×10^{-5} , a minimum value at 1×10^{-7} , and a decay period of 30. The first stage of training requires 50 epochs. The second stage of training requires 150 epochs. The mapping network and generator network of StyleGAN2 [15] are both frozen.

The user inputs handle points and target points on the initial image, which are then processed through the Latent Predictor and the Latent Regularizer, resulting in the edited image.

4.2 Qualitative Evaluation

Figure 2 illustrates the comparison between our method and DragGAN [22] under complex editing scenarios, while Figure 8 displays the comparison in simple editing scenarios. Figure 10 shows a comprehensive comparison of editing speed and image editing performance between our method and DragGAN [22]. Our method all outperforms DragGAN [22].

4.3 Quantitative Evaluation

Following the setup of DragGAN [22], we conducted a quantitative evaluation of our method, encompassing facial landmark manipulation and paired image reconstruction.

4.3.1 Face Landmark Manipulation. Following the setup of DragGAN [22], we employed an off-the-shelf tool, Dlib-ml [17], for facial landmark detection. Subsequently, we utilized a StyleGAN2 [15] pre-trained on the FFHQ [14] dataset to randomly generate two facial images, upon which we performed landmark detection. Our objective is to manipulate the landmarks of the first facial image to align them with the landmarks of the second facial image. Subsequently, we calculate the mean distance (MD) between the landmarks of the two images. The results are derived from an average of 2000 tests using the same set of test samples to evaluate all methods. In this manner, the final Mean Distance (MD) score reflects the efficacy of the method in moving the landmarks to the target positions. Evaluations were conducted with varying numbers of landmarks, including 1, 5, and 68. Additionally, we report the

Table 1: Quantitative evaluation on face landmark manipulation. We calculate the mean distance (MD) between the landmarks of the two images. The FID and Time are reported based on the ‘1 point’ setting. Red font indicates the best performance, while blue signifies the second best.

Method	1 point	5 points	68 points	FID	Time (s)
No edit	14.76	12.39	15.27	-	-
UserControllableLT	11.64	10.41	10.15	25.32	0.03
FreeGAN	1.45	3.03	4.17	7.67	2.0
DragGAN	1.62	3.23	4.32	8.30	1.9
Ours w/o Latent Regularizer	3.75	5.79	11.14	17.23	0.12
Ours w/o Latent Predictor	4.94	12.78	25.63	26.34	0.15
Ours	1.33	3.02	3.56	6.46	0.04

Fréchet Inception Distance (FID) scores between the edited images and the initial images.

The results are provided in Table 1. Our method achieves performance comparable to DragGAN [22] under different numbers of points. According to the FID scores, the image quality post-editing with our approach is superior. In terms of speed, our method significantly surpasses DragGAN [22]. Overall, our results are comparable to DragGAN [22], but with a faster execution speed.

4.3.2 Paired Image Reconstruction. In our study, both our method and DragGAN [22] were evaluated using the same settings as those employed in UserControllableLT [6]. In this study, we begin with a latent code w_1 and apply random perturbations to it in the same manner as described in UserControllableLT [6], thereby generating another latent code w_2 . Subsequently, we use these two latent codes to generate StyleGAN2 [15] images I_1 and I_2 , respectively. Following this, we calculate the optical flow between I_1 and I_2 and randomly select 32 pixel points from the flow field as user input U . Our research objective is to reconstruct image I_2 using only I_1 and U . The results are provided in Table 2. In most datasets, our approach demonstrates superior performance compared to DragGAN [22].

4.3.3 Ablation Study and Analysis Experiment. In this context, we investigate the roles of the Latent Regularizer and Latent Predictor in influencing the performance of the model. The results are provided in Table 1 and Table 2. ‘Ours w/o Latent Regularizer’ denotes the scenario where the Latent Regularizer is not utilized for the restoration of the latent codes. ‘Ours w/o Latent Predictor’ denotes the scenario where the length of latent code motion sequence, n , equals 1. Additionally, we discuss the impact of n on the effectiveness of the model trained in the final stage. The results are provided in Table 3.

4.3.4 Mean Distance Decay. We introduce a new metric, **Mean Distance Decay (MDD)**, to assess the speed performance of drag editing. MDD represents the ratio of the current mean distance between the handle points and the target points to the initial mean distance. A smaller value indicates a closer proximity between the handle points and the target points. The formula is as follows:

$$MDD = \frac{MD_{cur}}{MD_{init}} \quad (15)$$

where MD_{cur} represents the mean distance at the current moment, while MD_{init} denotes the initial mean distance.

As illustrated in the Figure 9, our approach demonstrates faster convergence in drag operations across various datasets compared

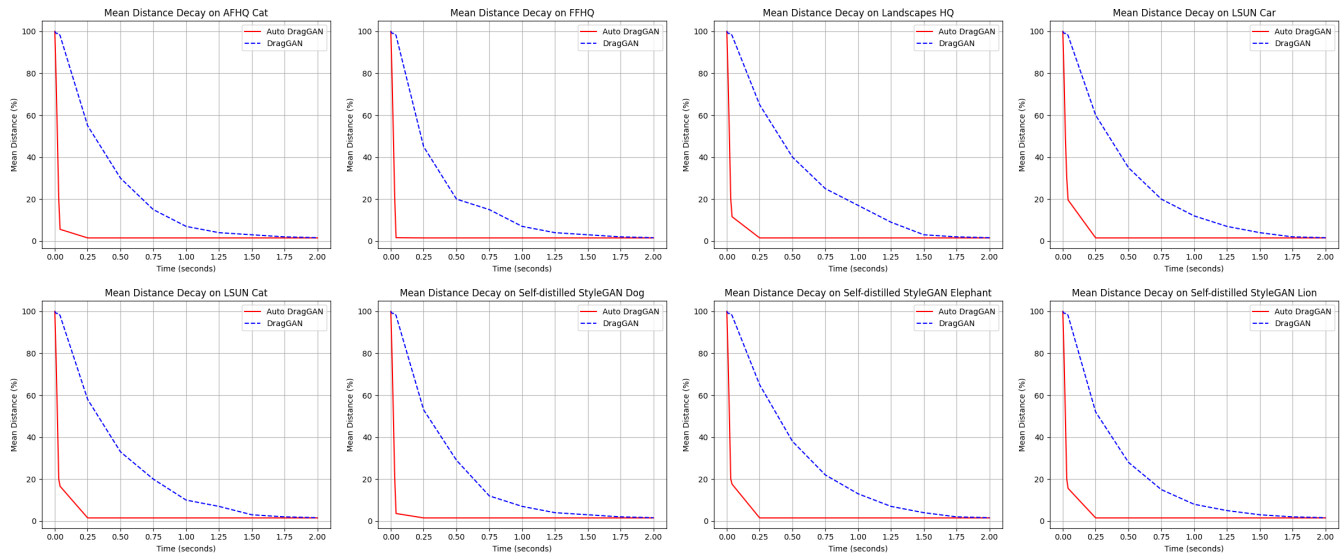


Figure 9: A comparative analysis of the Mean Distance Decay between Auto DragGAN and DragGAN [22] across various datasets. Auto DragGAN demonstrates faster convergence compared to DragGAN [22]. The convergence point at 2s indicates that both methods have comparable abilities in dragging the handle points to the target points.

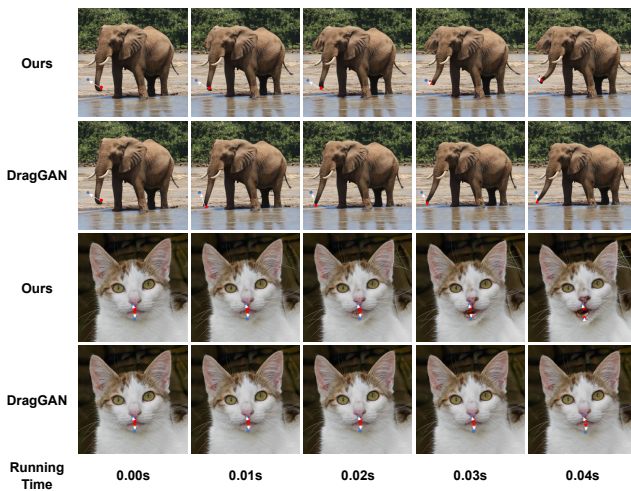


Figure 10: A qualitative comparison between our method and DragGAN [22] in terms of inference speed and image editing performance.

to DragGAN [22]. Our method begins to converge at approximately **0.04s** across various datasets, whereas DragGAN [22] starts to converge around **2s**. The calculation of **Mean Distance Decay (MDD)** is based on selecting only a single pair of handle point and target point. We calculated the **Mean Distance Decay (MDD)** on each dataset. We selected a handle point and a target point on the initial image, and then performed a drag operation to calculate the **Mean Distance Decay (MDD)** for both methods. As illustrated in the Figure 9, the final experimental results indicate that our method

Table 2: Quantitative evaluation on paired image reconstruction. We follow the evaluation in UserControllableLT [6] and report MSE ($\times 10^2$) \downarrow and LPIPS ($\times 10$) \downarrow scores. Red font indicates the best performance, while blue signifies the second best.

Dataset	Lion		LSUN Cat		Dog		LSUN Car	
	MSE	LPIPS	MSE	LPIPS	MSE	LPIPS	MSE	LPIPS
UserControllableLT	1.82	1.14	1.25	0.87	1.23	0.92	1.98	0.85
DragGAN	0.52	0.70	0.88	0.86	0.39	0.42	1.75	0.77
FreeGAN	0.48	0.67	0.79	0.96	0.38	0.37	1.64	0.64
Ours w/o Latent Regularizer	1.52	1.38	1.33	0.83	0.94	0.83	2.01	0.94
Ours	1.74	1.12	1.51	0.95	1.97	0.93	2.13	0.98
Ours	0.42	0.58	0.70	0.63	0.31	0.32	1.53	0.58

Table 3: Effects of n . Paired image reconstruction on Dog dataset. We follow the evaluation in UserControllableLT [6] and report MSE ($\times 10^2$) \downarrow score.

n	1	2	3	4	5	7	9	10
MSE	1.97	1.18	0.68	0.54	0.37	0.39	0.39	0.38

converges more rapidly than DragGAN [22], while maintaining a comparable dragging capability with DragGAN [22].

5 Conclusion

We propose Auto DragGAN, which, unlike DragGAN [22], FreeDrag [19], and DragDiffusion [27] that optimize latent vectors, is an autoregression-based model we have developed to learn the movement paths of latent codes within the latent space. Our method benefits from learning the variation patterns of latent codes during the image dragging process, and it significantly outperforms other methods [19, 22, 27] in handling complex dragging scenarios. This approach not only matches but slightly exceeds the effectiveness of DragGAN [22] while significantly boosting processing speed.

Acknowledgments

This work was supported by National Science and Technology Major Project(2021ZD0114600) ,National Natural Science Foundation of China (No. 62276260,62076235).

References

- [1] JiaWang Bian, Wen-Yan Lin, Yasuyuki Matsushita, Sai-Kit Yeung, Tan-Dat Nguyen, and Ming-Ming Cheng. 2017. Gms: Grid-based motion statistics for fast, ultra-robust feature correspondence. In *Proceedings of the IEEE conference on computer vision and pattern recognition*. 4181–4190.
- [2] Tim Brooks, Aleksander Holynski, and Alexei A Efros. 2023. Instructpix2pix: Learning to follow image editing instructions. In *Proceedings of the IEEE/CVF Conference on Computer Vision and Pattern Recognition*. 18392–18402.
- [3] Wenshuo Chen, Hongru Xiao, Erhang Zhang, Lijie Hu, Lei Wang, Mengyuan Liu, and Chen Chen. 2024. SATO: Stable Text-to-Motion Framework. arXiv:2405.01461 [cs.CV] <https://arxiv.org/abs/2405.01461>
- [4] Yunjey Choi, Youngjung Uh, Jaejun Yoo, and Jung-Woo Ha. 2020. Stargan v2: Diverse image synthesis for multiple domains. In *Proceedings of the IEEE/CVF conference on computer vision and pattern recognition*. 8188–8197.
- [5] Antonia Creswell, Tom White, Vincent Dumoulin, Kai Arulkumaran, Biswa Sengupta, and Anil A Bharath. 2018. Generative adversarial networks: An overview. *IEEE signal processing magazine* 35, 1 (2018), 53–65.
- [6] Yuki Endo. 2022. User-Controllable Latent Transformer for StyleGAN Image Layout Editing. In *Computer Graphics Forum*, Vol. 41. Wiley Online Library, 395–406.
- [7] Jianglin Fu, Shikai Li, Yuming Jiang, Kwan-Yee Lin, Chen Qian, Chen Change Loy, Wayne Wu, and Ziwei Liu. 2022. Stylegan-human: A data-centric odyssey of human generation. In *European Conference on Computer Vision*. Springer, 1–19.
- [8] Ian Goodfellow, Jean Pouget-Abadie, Mehdi Mirza, Bing Xu, David Warde-Farley, Sherjil Ozair, Aaron Courville, and Yoshua Bengio. 2014. Generative adversarial nets. *Advances in neural information processing systems* 27 (2014).
- [9] Zhaopeng Gu, Bingke Zhu, Guibo Zhu, Yingying Chen, Hao Li, Ming Tang, and Jinqiao Wang. 2024. FiLo: Zero-Shot Anomaly Detection by Fine-Grained Description and High-Quality Localization. *arXiv preprint arXiv:2404.13671* (2024).
- [10] Amir Hertz, Ron Mokady, Jay Tenenbaum, Kfir Aberman, Yael Pritch, and Daniel Cohen-Or. 2022. Prompt-to-prompt image editing with cross attention control. *arXiv preprint arXiv:2208.01626* (2022).
- [11] Jonathan Ho, Ajay Jain, and Pieter Abbeel. 2020. Denoising diffusion probabilistic models. *Advances in neural information processing systems* 33 (2020), 6840–6851.
- [12] Tero Karras, Miika Aittala, Janne Hellsten, Samuli Laine, Jaakko Lehtinen, and Timo Aila. 2020. Training generative adversarial networks with limited data. *Advances in neural information processing systems* 33 (2020), 12104–12114.
- [13] Tero Karras, Miika Aittala, Samuli Laine, Erik Härkönen, Janne Hellsten, Jaakko Lehtinen, and Timo Aila. 2021. Alias-free generative adversarial networks. *Advances in Neural Information Processing Systems* 34 (2021), 852–863.
- [14] Tero Karras, Samuli Laine, and Timo Aila. 2019. A style-based generator architecture for generative adversarial networks. In *Proceedings of the IEEE/CVF conference on computer vision and pattern recognition*. 4401–4410.
- [15] Tero Karras, Samuli Laine, Miika Aittala, Janne Hellsten, Jaakko Lehtinen, and Timo Aila. 2020. Analyzing and improving the image quality of stylegan. In *Proceedings of the IEEE/CVF conference on computer vision and pattern recognition*. 8110–8119.
- [16] Bahjat Kawar, Shiran Zada, Oran Lang, Omer Tov, Huiwen Chang, Tali Dekel, Inbar Mosseri, and Michal Irani. 2023. Imagic: Text-based real image editing with diffusion models. In *Proceedings of the IEEE/CVF Conference on Computer Vision and Pattern Recognition*. 6007–6017.
- [17] Davis E King. 2009. Dlib-ml: A machine learning toolkit. *The Journal of Machine Learning Research* 10 (2009), 1755–1758.
- [18] Diederik P Kingma and Max Welling. 2013. Auto-encoding variational bayes. *arXiv preprint arXiv:1312.6114* (2013).
- [19] Pengyang Ling, Lin Chen, Pan Zhang, Huaian Chen, and Yi Jin. 2023. Freedrag: Point tracking is not you need for interactive point-based image editing. *arXiv preprint arXiv:2307.04684* (2023).
- [20] Ron Mokady, Amir Hertz, Kfir Aberman, Yael Pritch, and Daniel Cohen-Or. 2023. Null-text inversion for editing real images using guided diffusion models. In *Proceedings of the IEEE/CVF Conference on Computer Vision and Pattern Recognition*. 6038–6047.
- [21] Ron Mokady, Omer Tov, Michal Yarom, Oran Lang, Inbar Mosseri, Tali Dekel, Daniel Cohen-Or, and Michal Irani. 2022. Self-distilled stylegan: Towards generation from internet photos. In *ACM SIGGRAPH 2022 Conference Proceedings*. 1–9.
- [22] Xingang Pan, Ayush Tewari, Thomas Leimkühler, Lingjie Liu, Abhimitra Meka, and Christian Theobalt. 2023. Drag your gan: Interactive point-based manipulation on the generative image manifold. In *ACM SIGGRAPH 2023 Conference Proceedings*. 1–11.
- [23] Gaurav Parmar, Krishna Kumar Singh, Richard Zhang, Yijun Li, Jingwan Lu, and Jun-Yan Zhu. 2023. Zero-shot image-to-image translation. In *ACM SIGGRAPH 2023 Conference Proceedings*. 1–11.
- [24] Alec Radford, Luke Metz, and Soumith Chintala. 2015. Unsupervised representation learning with deep convolutional generative adversarial networks. *arXiv preprint arXiv:1511.06434* (2015).
- [25] Daniel Roich, Ron Mokady, Amit H Bermano, and Daniel Cohen-Or. 2022. Pivotal tuning for latent-based editing of real images. *ACM Transactions on graphics (TOG)* 42, 1 (2022), 1–13.
- [26] Robin Rombach, Andreas Blattmann, Dominik Lorenz, Patrick Esser, and Björn Ommer. 2022. High-resolution image synthesis with latent diffusion models. In *Proceedings of the IEEE/CVF conference on computer vision and pattern recognition*. 10684–10695.
- [27] Yujun Shi, Chuhui Xue, Jiachun Pan, Wenqing Zhang, Vincent YF Tan, and Song Bai. 2023. DragDiffusion: Harnessing Diffusion Models for Interactive Point-based Image Editing. *arXiv preprint arXiv:2306.14435* (2023).
- [28] Ivan Skorokhodov, Grigori Sotnikov, and Mohamed Elhoseiny. 2021. Aligning latent and image spaces to connect the unconnectable. In *Proceedings of the IEEE/CVF International Conference on Computer Vision*. 14144–14153.
- [29] Jascha Sohl-Dickstein, Eric Weiss, Niru Maheswaranathan, and Surya Ganguli. 2015. Deep unsupervised learning using nonequilibrium thermodynamics. In *International conference on machine learning*. PMLR, 2256–2265.
- [30] Jiaming Song, Chenlin Meng, and Stefano Ermon. 2020. Denoising diffusion implicit models. *arXiv preprint arXiv:2010.02502* (2020).
- [31] Yang Song, Jascha Sohl-Dickstein, Diederik P Kingma, Abhishek Kumar, Stefano Ermon, and Ben Poole. 2020. Score-based generative modeling through stochastic differential equations. *arXiv preprint arXiv:2011.13456* (2020).
- [32] Aäron Van Den Oord, Nal Kalchbrenner, and Koray Kavukcuoglu. 2016. Pixel recurrent neural networks. In *International conference on machine learning*. PMLR, 1747–1756.
- [33] Ashish Vaswani, Noam Shazeer, Niki Parmar, Jakob Uszkoreit, Llion Jones, Aidan N Gomez, Łukasz Kaiser, and Illia Polosukhin. 2017. Attention is all you need. *Advances in neural information processing systems* 30 (2017).
- [34] Fisher Yu, Ari Seff, Yinda Zhang, Shuran Song, Thomas Funkhouser, and Jianxiong Xiao. 2015. Lsun: Construction of a large-scale image dataset using deep learning with humans in the loop. *arXiv preprint arXiv:1506.03365* (2015).